Stern-Gerlach effect of weak-light ultraslow vector solitons

Chao Hang and Guoxiang Huang[*]

State Key Laboratory of Precision Spectroscopy and Department of Physics, East China Normal University, Shanghai 200062, China
(Received 20 June 2012; revised manuscript received 5 September 2012; published 5 October 2012)

We propose a scheme to exhibit Stern-Gerlach deflection of high-dimensional vector optical solitons at a weak-light level in a cold atomic gas via electromagnetically induced transparency. We show that the propagating velocity and generation power of such solitons can be reduced to 10^{-6} c (c is light speed in vacuum) and lowered to magnitude of nanowatt, respectively. The stabilization of the solitons is realized by using an optical lattice potential formed by a far-detuned laser field, and trajectories of them are deflected significantly by using a transversal Stern-Gerlach gradient magnetic field. Deflection angles of the solitons can be of magnitude of 10^{-3} rad when propagating several millimeters. Different from atomic Stern-Gerlach deflection, deflection angles of the solitons can be distinct for different polarization components and can be manipulated in a controllable way. The result obtained can be described in terms of the Stern-Gerlach effect for vector optical solitons with quasispin and effective magnetic moment.

I. INTRODUCTION

The Stern-Gerlach (SG) effect, that is, particles with nonzero magnetic moments deflect when passing through an inhomogeneous magnetic field, was first discovered in the early period of quantum mechanics. This effect illustrates in a drastic manner the necessity for a radical departure from classical mechanics, and characterizes quantum mechanics in a simple and fundamental way [1]. Recently, a similar effect was also predicted in many other systems such as spinor Fermi and Bose gases in tight atom waveguides [2], and mixed left- and right-handed chiral molecules [3].

All known massive elementary particles, such as electrons and protons, have nonzero magnetic moments. In contrast, photons have no magnetic moment in vacuum, and hence experience no force when passing through an inhomogeneous magnetic field. Recently, in a very remarkable experiment [4], Karpa and Weitz demonstrated that photons can acquire an effective magnetic moment when propagating in a resonant atomic gas, and hence can deflect in a gradient magnetic field. For obtaining a significant deflection angle, they exploited electromagnetically induced transparency (EIT) [5], by which a very small absorption and very slow propagating velocity of light can be realized.

However, the EIT-enhanced deflection of light in Ref. [4] cannot be explained as a standard SG effect because only one component of "spin" is involved. In the present work we propose a double EIT scheme to demonstrate the SG effect of high-dimensional ultraslow vector optical soliton (VOS), which not only has two polarization components (i.e., a quasispin) but also allows a distortionless propagation.

Before proceeding we note that besides Ref. [4] the optical beam deflection in external fields has been the subject of many previous works [6–11]. The present work is related to Refs. [4,9,10] and to the recent study of weak-light solitons [12–18]. The essence of Refs. [4,9,10] is the SG effect of linear polaritons via EIT. However, such linear polaritons spread and attenuate during propagation because of the existence of diffraction and other detrimental effects. In Refs. [12–18], weak-light solitons via EIT are suggested, but no SG deflection of them have been considered.

In contrast with all previous works, the scheme presented here exploits EIT-enhanced Kerr nonlinearity, which allows the formation and propagation of high-dimensional VOS, or called *nonlinear polariton*, with intrinsic quasispin and effective magnetic moment. We find that the propagating velocity and generation power of the VOS can be reduced to 10^{-6} c (c is light speed in vacuum) and lowered to a magnitude of a nanowatt, respectively. We demonstrate that the stabilization of the VOS can be realized by using an optical lattice potential formed by a far-detuned laser field, and trajectories of them can be deflected significantly by using a transversal Stern-Gerlach gradient magnetic field. Deflection angles of the VOS can be of the magnitude of 10^{-3} rad when propagating several millimeters. Different from atomic Stern-Gerlach deflection, deflection angles of the VOS can be distinct for different polarization components and can be manipulated in a controllable way. Because the SG deflection of the nonlinear polariton does not spread and attenuate for a long propagation distance, the present scheme, compared with the linear ones [4,9,10], is more efficient and robust for the observation of the SG effect of photons as well as for practical (e.g., magnetometery) applications.

The rest of the article is arranged as follows. In Sec. II the theoretical model under study is introduced. In Sec. III linear dispersion and absorption properties of the system are analyzed. In Sec. IV nonlinear envelope equations are derived by using a method of multiple scales, and ultraslow vector optical soliton solutions at very low light level are obtained. In Sec. V the Stern-Gerlach effect of ultraslow vector optical solitons is studied. Finally, in the last section a summary of the main results obtained in this work is given.

II. MODEL AND LINEAR DISPERSION RELATION

We consider a medium consisting of five-level atoms with M configuration. A linearly polarized, pulsed probe field (with pulse duration τ_0) $\mathbf{E}_p = \mathbf{E}_{p1} + \mathbf{E}_{p2} = (\hat{\epsilon}_- \mathcal{E}_{p1} + \hat{\epsilon}_+ \mathcal{E}_{p2})$
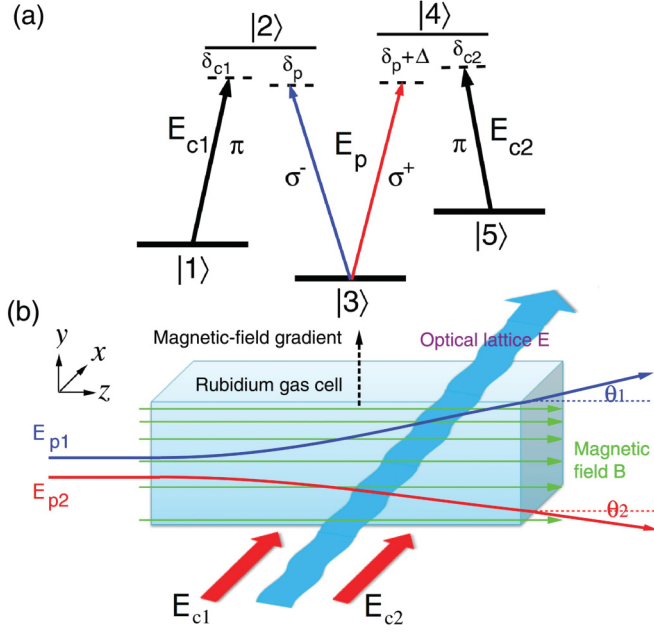
————
[*]gxhuang@phys.ecnu.edu.cn

FIG. 1. (Color online) (a) Double EIT scheme. $\mathbf{E}_p$ and $\mathbf{E}_{cj}$ ($j = 1,2$) are probe and control fields, respectively; δ_p, $\delta_p + \Delta$, and δ_{cj} are detunings. (b) A possible experimental arrangement, where an inhomogeneous static magnetic field $\mathbf{B}(y) = \hat{\mathbf{z}}(B_0 + B_1 y)$ removes the degeneracy of ground states $|j\rangle$ ($j = 1,3,5$) and excited states $|l\rangle$ ($l = 2,4$), and causes Stern-Gerlach deflection of probe-field components. θ_1 and θ_2 are, respectively, deflection angles of σ^- polarization component (i.e., $\mathbf{E}_{p1}$) and σ^+ polarization component (i.e., $\mathbf{E}_{p2}$) of high-dimensional vector optical soliton, which has a quasispin and an effective magnetic moment. The curved thick arrow represents the far-detuned optical lattice field $\mathbf{E}(x,t) = \hat{\mathbf{x}} E_0 \cos[x/(2R_\perp)] \cos(\omega_L t)$ used to stabilize the soliton.

$\exp[i(k_p z - \omega_p t)] + $ c.c. drives the transitions $|3\rangle \leftrightarrow |2\rangle$ and $|3\rangle \leftrightarrow |4\rangle$ by its left-circular (i.e., σ^-) polarization component $\mathbf{E}_{p1}$ and right-circular (i.e., σ^+) polarization component $\mathbf{E}_{p2}$, respectively. Here $\hat{\epsilon}_- \equiv (\hat{\mathbf{x}} - i\hat{\mathbf{y}})/\sqrt{2}$ and $\mathcal{E}_{p1}$ [$\hat{\epsilon}_+ \equiv (\hat{\mathbf{x}} + i\hat{\mathbf{y}})/\sqrt{2}$ and $\mathcal{E}_{p2}$] are, respectively, the unit vector and envelope of the σ^- (σ^+) polarization component. A π-polarized continuous-wave control field $\mathbf{E}_{c1} = \hat{\mathbf{z}}\mathcal{E}_{c1} \exp[i(k_{c1}x - \omega_{c1}t)] + $ c.c. {$\mathbf{E}_{c2} = \hat{\mathbf{z}}\mathcal{E}_{c2} \exp[i(k_{c2}x - \omega_{c2}t)] + $ c.c.} drives the transition $|1\rangle \leftrightarrow |2\rangle$ ($|5\rangle \leftrightarrow |4\rangle$) [Fig. 1(a)]. $\hat{\mathbf{x}}$, $\hat{\mathbf{y}}$, and $\hat{\mathbf{z}}$ are unit vectors along coordinate axes x, y, and z, respectively [Fig. 1(b)]. The control field envelopes $\mathcal{E}_{c1}$ and $\mathcal{E}_{c2}$ are strong enough so that they are taken to be undepleted during the evolution of the probe field.

We assume an inhomogeneous static magnetic field

$$\mathbf{B}(y) = \hat{\mathbf{z}}B(y) = \hat{\mathbf{z}}(B_0 + B_1 y), \tag{1}$$

with $B_1 \ll B_0$ is applied to the medium. Here B_0 contributes to a Zeeman level shift $\Delta E_{\text{Zeeman}} = \mu_B g_F^j m_F^j B_0$, and hence removes the degeneracy of ground-state sublevels $|j\rangle$ ($j = 1,3,5$) and the excited-state sublevels $|l\rangle$ ($l = 2,4$). μ_B, g_F^j, and m_F^j are Bohr magneton, gyromagnetic factor, and magnetic quantum number of the level $|j\rangle$, respectively. B_1 is a transverse gradient magnetic field, which results in SG deflection of the polarization components of the probe field.

We assume further a small, far-detuned laser field

$$\mathbf{E}(x,t) = \hat{\mathbf{x}} E_0 \cos(x/R_\perp) \cos(\omega_L t) \tag{2}$$

is also applied into the system, where E_0, $R_\perp$, and ω_L are field amplitude, beam radius, and angular frequency, respectively. Due to $\mathbf{E}(x,t)$, Stark level shift $\Delta E_{j,\text{Stark}} = -\frac{1}{2}\alpha_j\langle E^2\rangle_t = -\frac{1}{2}\alpha_j E^2(x)$ occurs. Here α_j is the scalar polarizability of the level $|j\rangle$, $\langle O(t)\rangle_t$ denotes the time average in an oscillation cycle for the quantity $O(t)$, and hence we have $E(x) = (E_0/\sqrt{2})\cos(x/R_\perp)$. The aim of introducing the far-detuned laser field is to form a low-dimensional optical lattice to stabilize the high-dimensional VOS without losing its mobility [19], as shown below. In addition, atoms are assumed prepared initially in the ground-state level $|3\rangle$ and trapped in a gas cell with ultracold temperature to cancel Doppler broadening and collisions. Thus, the system is composed of two Λ-type configurations. A possible arrangement of experimental apparatus is suggested in Fig. 1(b).

Under electric-dipole and rotating-wave approximations, the Hamiltonian of the system in interaction picture is

$$
\begin{aligned}
H_{\text{int}}/\hbar &= (\delta_p - \delta_{c1})|1\rangle\langle 1| + \delta_p|2\rangle\langle 2| + (\delta_p + \Delta)|4\rangle\langle 4| \\
&\quad + (\delta_p + \Delta - \delta_{c2})|5\rangle\langle 5| + \Omega_{c1}|2\rangle\langle 1| + \Omega_{p1}|2\rangle\langle 3| \\
&\quad + \Omega_{p2}|4\rangle\langle 3| + \Omega_{c2}|4\rangle\langle 5| + \text{H.c.},
\end{aligned}
\tag{3}
$$

where $\Omega_{p1} = -(\mathbf{p}_{23} \cdot \hat{\epsilon}_-)\mathcal{E}_{p1}/\hbar$, $\Omega_{p2} = -(\mathbf{p}_{43} \cdot \hat{\epsilon}_+)\mathcal{E}_{p2}/\hbar$ ($\Omega_{c1} = -(\mathbf{p}_{21} \cdot \hat{\mathbf{z}})\mathcal{E}_{c1}/\hbar$, and $\Omega_{c2} = -(\mathbf{p}_{45} \cdot \hat{\mathbf{z}})\mathcal{E}_{c2}/\hbar$) are, respectively, Rabi frequencies of two circularly polarized components of the probe field (two π-polarized control fields), with $\mathbf{p}_{jl}$ being the electric dipole matrix element associated with the transition from $|j\rangle$ to $|l\rangle$. Detunings are defined as $\delta_p = \omega_{23} + \mu_{23}B(y) - \frac{1}{2}\alpha_{23}E(x)^2 - \omega_p$, $\delta_{c1} = \omega_{21} + \mu_{21}B(y) - \frac{1}{2}\alpha_{21}E(x)^2 - \omega_{c1}$, $\delta_{c2} = \omega_{45} + \mu_{45}B(y) - \frac{1}{2}\alpha_{45}E(x)^2 - \omega_{c2}$, and $\Delta = \mu_{42}B(y) - \frac{1}{2}\alpha_{42}E(x)^2$, where $\mu_{jl} = \mu_B(g_F^j m_F^j - g_F^l m_F^l)/\hbar$, $\alpha_{jl} = (\alpha_j - \alpha_l)/\hbar$, and $\omega_{jl} = (E_j - E_l)/\hbar$ with E_j being the eigenenergy of the state $|j\rangle$.

The motion of atoms is governed by the Bloch equation for density-matrix ρ:

$$\partial\rho/\partial t = -i[H_{\text{int}},\rho]/\hbar - \Gamma(\rho), \tag{4}$$

where $\Gamma(\rho)$ is a relaxation matrix representing spontaneous emission and dephasing. The explicit form of Eq. (4) is given in Appendix A.

The evolution of electric field is controlled by Maxwell equation $\nabla^2\mathbf{E} - (1/c^2)\partial^2\mathbf{E}/\partial t^2 = (1/\epsilon_0 c^2)\partial^2\mathbf{P}/\partial t^2$, where $\mathbf{P} = \mathcal{N}\text{Tr}(\mathbf{p}\rho)$ is electric polarization with $\mathcal{N}$ the atomic concentration. Under slowly varying envelope approximation, the Maxwell equation reduces to equations for Ω_{p1}, Ω_{p2}:

$$\left[i\left(\frac{\partial}{\partial z} + \frac{1}{c}\frac{\partial}{\partial t}\right) + \frac{c\nabla_\perp^2}{2\omega_p}\right]\Omega_{p1,p2} - \kappa_{32,34}\rho_{23,43} = 0, \tag{5}$$

where $\nabla_\perp^2 = \partial^2/\partial x^2 + \partial^2/\partial y^2$ and $\kappa_{32,34} = \mathcal{N}|\mathbf{p}_{32,34} \cdot \hat{\epsilon}_\mp|^2\omega_p/(2\hbar\epsilon_0 c)$ with ϵ_0 the vacuum dielectric constant.

If the diffraction effect are very weak, a linear propagation of the probe field can be obtained by taking $\Omega_{p1,p2}$ as small quantities and B_1, E_0 to be zero. Then from the Maxwell-Bloch
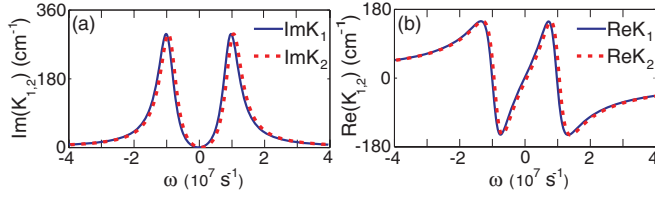
FIG. 2. (Color online) (a) $\mathrm{Im}K_j(\omega)$ and (b) $\mathrm{Re}K_j(\omega)$ as functions of ω. The solid and dotted lines correspond to the σ^- ($j=1$) and σ^+ ($j=2$) polarization components of the probe field, respectively.

(MB) Eqs. (4) and (5) one obtains the solution proportional to $\exp\{i[K_j(\omega)z - \omega t)]\}$ ($j=1,2$), with the linear dispersion relation [20]

$$K_{1,2}(\omega) = \frac{\omega}{c} + \kappa_{32,34}\frac{\omega - d_{1,5}}{D_{1,2}}. \qquad (6)$$

Here $D_{1,2} = |\Omega_{c1,c2}|^2 - (\omega - d_{1,5})(\omega - d_{2,4})$, $d_1 = (\delta_p - \delta_{c1}) - i\gamma_{13}/2$, $d_2 = \delta_p - i(\Gamma_2 + \gamma_{23})/2$, $d_4 = (\delta_p + \Delta) - i(\Gamma_4 + \gamma_{34})/2$, and $d_5 = (\delta_p + \Delta - \delta_{c2}) - i\gamma_{35}/2$ with $\delta_p = \omega_{23} + \mu_{23}B_0 - \omega_p$, $\Delta = \mu_{42}B_0$, $\delta_{c1} = \omega_{21} + \mu_{21}B_0 - \omega_{c1}$, and $\delta_{c2} = \omega_{45} + \mu_{45}B_0 - \omega_{c2}$. Γ_j and γ_{jl} denote the spontaneous emission and dephasing rates of relevant states, respectively.

From Eq. (6) we see that the linear dispersion relation of the system has two branches. Figures 2(a) and 2(b) show the imaginary part [$\mathrm{Im}K_j(\omega)$] and real part [$\mathrm{Re}K_j(\omega)$] of $K_j(\omega)$ ($j=1,2$) as functions of frequency ω, respectively. The parameters are chosen from a laser-cooled ^{85}Rb atomic gas with atomic states assigned as $|1\rangle = |5^2 S_{1/2}, F = 2, m_F = -1\rangle$, $|2\rangle = |5^2 P_{1/2}, F = 2, m_F = -1\rangle$, $|3\rangle = |5^2 S_{1/2}, F = 1, m_F = 0\rangle$, $|4\rangle = |5^2 P_{1/2}, F = 2, m_F = 1\rangle$, and $|5\rangle = |5^2 S_{1/2}, F = 2, m_F = 1\rangle$. The decay rates are $\Gamma_2 \simeq \Gamma_4 \simeq 6$ MHz and $\gamma_{13} \simeq \gamma_{23} \simeq \gamma_{34} \simeq \gamma_{35} \simeq 50$ Hz. The other parameters are taken as $\kappa_{32} \simeq \kappa_{34} = 1.0 \times 10^9$ cm^{-1}s^{-1}, $\Omega_{c1} = \Omega_{c2} = 1.0 \times 10^7$ s^{-1}, $\delta_p = \delta_{c1} = \delta_{c2} = 0$, and $B_0 = 34.1$ mG. In both panels the solid (dotted) lines corresponds to σ^- (σ^+) polarization component of the probe field. From Fig. 2(a) we see that large and deep transparency windows in the absorption spectra of both polarization components appear, and they nearly coincide with each other. Such double EIT phenomenon results from the quantum destruction interference contributed by the two control fields. Furthermore, due to EIT, the group velocities of both components [defined by $V_{gj} = \mathrm{Re}(\partial K_j/\partial\omega)^{-1}$] become very small compared with c and well matched [see Fig. 2(b)]. Indeed, using the above parameters we obtain

$$V_{g1} \simeq V_{g2} \simeq 3.3 \times 10^{-6}c. \qquad (7)$$

Such ultraslow, matched group velocity is very crucial for obtaining significant SG deflection of the probe field.

III. NONLINEAR ENVELOPE EQUATIONS AND VECTOR OPTICAL SOLITONS

The linear propagation is unstable due to the diffraction and other detrimental effects, which results in spreading and attenuation of the probe field during propagation, as explicitly demonstrated by Eq. (24) in Ref. [10]. To solve this problem

we suggest to use nonlinear effect to suppress the spreading and attenuation and hence obtain a probe pulse that is robust during propagation.

Now we employ the method of multiple scales [13] to derive nonlinear envelope equations of the probe-field components. To this aim, we take the following asymptotic expansions $\rho_{mm} = \sum_{l=1}^{\infty} \epsilon^l \rho_{mm}^{(l)}$ ($m = 1, 2, 4, 5$), $\rho_{33} = 1 + \sum_{l=1}^{\infty} \epsilon^l \rho_{33}^{(l)}$, $\rho_{mn} = \sum_{l=1}^{\infty} \epsilon^l \rho_{mn}^{(l)}$ ($m, n = 1$–5; $m \neq n$), and $\Omega_{pj} = \sum_{l=1}^{\infty} \epsilon^l \Omega_{pj}^{(l)}$ ($j = 1, 2$). Here ϵ is a small parameter characterizing the small population depletion of the ground state, and all quantities on the right-hand side of asymptotic expansions are considered as functions of multiscale variables $z_l = \epsilon^l z$ ($l = 0, 2$), $(x_1, y_1) = \epsilon(x, y)$, and $t_l = \epsilon^l t$ ($l = 0, 2$).

The inhomogeneous static magnetic field and the far-detuned laser field [given respectively by Eqs. (1) and (2)] are now assumed to be $B(y_1) = B_0 + \epsilon^2 B_1 y_1$ and $E(x_1) = \epsilon(E_0/\sqrt{2})\cos(x_1/R_\perp)$. Thus, detunings can be expanded as $\delta_p = \delta_p^{(0)} + \epsilon^2 \delta_p^{(2)}, \Delta = \Delta^{(0)} + \epsilon^2 \Delta^{(2)}, \delta_{c1} = \delta_{c1}^{(0)} + \epsilon^2 \delta_{c1}^{(2)}$, and $\delta_{c2} = \delta_{c2}^{(0)} + \epsilon^2 \delta_{c2}^{(2)}$, where $\delta_p^{(0)} = \omega_{23} + \mu_{23}B_0 - \omega_p$, $\Delta^{(0)} = \mu_{42}B_0$, $\delta_{c1}^{(0)} = \omega_{21} + \mu_{21}B_0 - \omega_{c1}$, $\delta_{c2}^{(0)} = \omega_{45} + \mu_{45}B_0 - \omega_{c2}$, $\delta_p^{(2)} = \mu_{23}B_1 y_1 - \frac{1}{4}\alpha_{23}E_0^2 \cos^2(x_1/R_\perp)$, $\Delta^{(2)} = \mu_{42}B_1 y_1 - \frac{1}{4}\alpha_{42}E_0^2 \cos^2(x_1/R_\perp), \delta_{c1}^{(2)} = \mu_{21}B_1 y_1 - \frac{1}{4}\alpha_{21}E_0^2 \cos^2(x_1/R_\perp)$, and $\delta_{c2}^{(2)} = \mu_{45}B_1 y_1 - \frac{1}{4}\alpha_{45}E_0^2 \cos^2(x_1/R_\perp)$. Note that detunings at the leading order are homogeneous in space, whereas detunings at the second order have spatial distributions which depend on B_1 (the SG gradient magnetic field) and E_0 (the far-detuned laser field).

Substituting above expansions into the MB Eqs. (4) and (5) we obtain a chain of linear, but inhomogeneous equations (the explicit forms of them are given in Appendix B), which can be solved order by order.

At the first order ($l = 1$) we obtain the solution for the probe field

$$\Omega_{pj}^{(1)} = F_j \exp\{i[K_j(\omega)z_0 - \omega t_0)]\}, \qquad (8)$$

where F_j are yet to be determined envelope functions of slow variables z_2 and t_2, and $K_j(\omega)$ is given by the linear dispersion relation (6) with $d_1 = \delta_p^{(0)} - \delta_{c1}^{(0)} - i\gamma_{13}/2$, $d_2 = \delta_p^{(0)} - i(\Gamma_2 + \gamma_{23})/2$, $d_4 = \delta_p^{(0)} + \Delta^{(0)} - i(\Gamma_4 + \gamma_{34})/2$, and $d_5 = \delta_p^{(0)} + \Delta^{(0)} - \delta_{c2}^{(0)} - i\gamma_{35}/2$ in D_j. Solutions of density-matrix elements at this order read $\rho_{13}^{(1)} = -\Omega_{c1}^* \Omega_{p1}^{(1)}/D_1$, $\rho_{23}^{(1)} = -(\omega - d_1)\Omega_{p1}^{(1)}/D_1$, $\rho_{34}^{(1)} = -(\omega - d_5^*)\Omega_{p2}^{*(1)}/D_2^*$, $\rho_{35}^{(1)} = -\Omega_{c2}\Omega_{p2}^{*(1)}/D_2^*$, with the other density-matrix elements being zero.

At the second order ($l = 2$), one obtains the expressions of $\rho_{mm}^{(1)}$ ($m = 1$–5), $\rho_{12}^{(1)}, \rho_{14}^{(1)}, \rho_{15}^{(1)} \rho_{24}^{(1)}, \rho_{25}^{(1)}, \rho_{45}^{(1)}$, which are lengthy and hence omitted here. The other second-order density-matrix elements are zero.

At the third order ($l = 3$), a solvability condition for $\Omega_{pj}^{(3)}$ gives the governing equations for the envelope functions F_j ($j = 1, 2$):

$$i\left(\frac{\partial}{\partial z_2} + \frac{1}{V_{g1,g2}}\frac{\partial}{\partial t_2}\right)F_{1,2} + \frac{c\bar{\nabla}_\perp^2}{2\omega_p}F_{1,2} - (W_{11,22}|F_{1,2}|^2$$
$$+ W_{12,21}|F_{2,1}|^2)e^{-2\bar{a}_{1,2}z_2}F_{1,2} + [M_{1,2}B_{1,2}y_1 + N_{1,2}E_0^2$$
$$\times \cos^2(x_1/R_\perp)]F_{1,2} = 0, \qquad (9)$$

where $\bar{\nabla}_\perp^2 = \partial^2/\partial x_1^2 + \partial^2/\partial y_1^2$, and

$$V_{g1,g2} = \left\{ \frac{1}{c} + \kappa_{32,34} \frac{|\Omega_{c1,c2}|^2 + (\omega + d_{1,5})^2}{D_{1,2}^2} \right\}^{-1}, \quad (10a)$$

$$W_{11,22} = -\kappa_{32,34} d_{1,5} \frac{|d_{1,5}|^2 + |\Omega_{c1,c2}|^2}{D_{1,2}|D_{1,2}|^2}, \quad (10b)$$

$$W_{12,21} = -\kappa_{32,34} d_{1,5} \frac{|d_{5,1}|^2 + |\Omega_{c2,c1}|^2}{D_{1,2}|D_{2,1}|^2}, \quad (10c)$$

$$M_{1,2} = -\kappa_{32,34} \frac{d_{1,5}^2 \mu_{23,43} + |\Omega_{c1,c2}|^2 \mu_{13,53}}{D_{1,2}^2}, \quad (10d)$$

$$N_{1,2} = \kappa_{32,34} \frac{d_{1,5}^2 \alpha_{23,43} + |\Omega_{c1,c2}|^2 \alpha_{13,53}}{4D_{1,2}^2}, \quad (10e)$$

with $\bar{a}_j = \epsilon^{-2} \text{Im}[K_j(\omega = 0)]$.

After returning to original variables, Eq. (9) can be written into the dimensionless form

$$\left[i \left(\frac{\partial}{\partial s} + \frac{1}{v_{g1,g2}} \frac{\partial}{\partial \tau} \right) + \frac{1}{2} \left(\frac{\partial^2}{\partial \xi^2} + \frac{\partial^2}{\partial \eta^2} \right) \right] u_{1,2}$$
$$- (g_{11,22}|u_{1,2}|^2 + g_{12,21}|u_{2,1}|^2)u_{1,2} + V_{1,2}(\xi,\eta)u_{1,2}$$
$$= -i A_{1,2} u_{1,2}, \quad (11)$$

where we have introduced new dimensionless variables $s = z/L_{\text{Diff}}$, $\tau = t/\tau_0$, $(\xi,\eta) = (x,y)/R_\perp$, $v_{gj} = V_{gj}\tau_0/L_{\text{Diff}}$, and $u_j = (\Omega_{pj}/U_0)e^{-i\text{Re}[K_j|_{\omega=0}]z}$. Here $L_{\text{Diff}} \equiv \omega_p R_\perp^2/c$, τ_0, and U_0 are, respectively, typical diffraction length, probe-field pulse duration, and Rabi frequency; $g_{11,12,21,22} = W_{11,12,21,22}/|W_{22}|$ characterize, respectively, self-phase ($g_{11,22}$) and cross-phase ($g_{12,21}$) modulations; $A_j = \text{Im}[K_j|_{\omega=0}]L_{\text{Diff}}$ ($j = 1,2$) are small absorption coefficients contributed mainly by decay rates Γ_2 and Γ_4. The combined potentials in Eq. (11) have the form

$$V_j(\xi,\eta) = \mathcal{M}_j \eta + \mathcal{N}_j \cos^2(\xi), \quad (12)$$

where $\mathcal{M}_{1,2} = L_{\text{Diff}} M_{1,2} R_\perp B_1$ and $\mathcal{N}_{1,2} = L_{\text{Diff}} N_{1,2} E_0^2$ are the contributions from the SG gradient magnetic field (proportional to B_1) and the far-detuned optical lattice field (proportional to E_0^2), respectively.

In deriving Eq. (11) we have assumed τ_0 is large so that second-order dispersion (i.e., the term proportional to $\partial^2 u_j/\partial \tau^2$) can be neglected. This can be easily realized experimentally. In fact, when taking $\tau_0 = 2.1 \ \mu$s, $\delta_p = 1.0 \times 10^6$ s^{-1}, $\delta_{c2} = 1.0 \times 10^5$ s^{-1}, and $R_\perp = 16 \ \mu$m with other parameters the same as in Fig. 2, one has typical (second-order) dispersion length of the system $L_{\text{Disp}}[\equiv\tau_0^2/\text{Re}(d^2K_j/d\omega^2)|_{\omega=0}] \gtrsim 7.6$ cm, which is much larger than typical diffraction length L_{Diff} and nonlinearity length $L_{\text{Nonl}}[\equiv 1/(U_0^2|W_{22}|)]$, both of which are only 0.2 cm.

We seek the solutions of Eq. (11) with the form $u_j(\rho_j,\tau,\xi,\eta) = F_j(\rho_j)v_j(\tau,\xi,\eta)$, where $F_j(\rho_j)$ are normalized Gaussian functions, that is, $F_j = [1/(\rho_0\sqrt{\pi})]^{1/2} \exp[-\rho_j^2/(2\rho_0^2)]$ with $\rho_j = s - v_{gj}\tau$ and ρ_0 a constant [10]. Integrating out the variable ρ_j, Eq. (11)
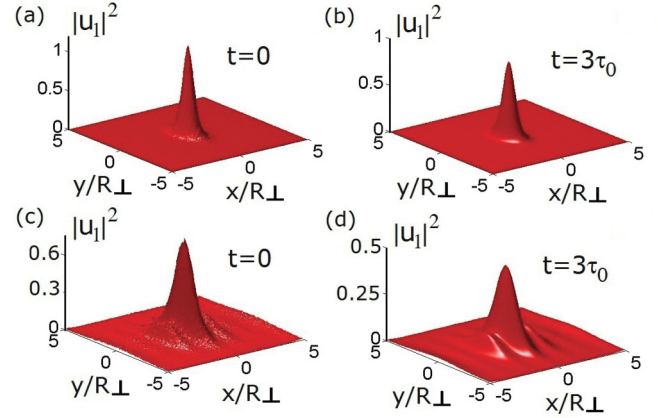

FIG. 3. (Color online) (a) and (b) Evolutions of $|u_1|^2$, respectively, at $t = 0$ and $t = 3\tau_0$ for the single-peaked VOS. (c) and (d) Evolutions of $|u_1|^2$, respectively, at $t = 0$ and $t = 3\tau_0$ for the multiple-peaked VOS. The SG gradient magnetic field is absent (i.e., $B_1 = 0$). The stability of the VOS is achieved by the far-detuned optical lattice. Result for $|u_2|^2$ is similar to that for $|u_1|^2$ thus not shown.

becomes

$$\left[\frac{i}{v_{g1,g2}} \frac{\partial}{\partial \tau} + \frac{1}{2} \left(\frac{\partial^2}{\partial \xi^2} + \frac{\partial^2}{\partial \eta^2} \right) \right] v_{1,2} - \frac{1}{\sqrt{2\pi}\rho_0} (g_{11,22}|v_{1,2}|^2$$
$$+ g_{12,21}|v_{2,1}|^2)v_{1,2} + V_{1,2}(\xi,\eta)v_{1,2} = -i A_{1,2} v_{1,2}. \quad (13)$$

Shown in Figs. 3(a) and 3(b) are, respectively, results of numerical simulation for $|u_1|^2$ at $t = 0$ and $t = 3\tau_0$ for a deep optical lattice (by taking $E_0 = 4.5 \times 10^4$ V cm^{-1}). The soliton obtained displays a single-peaked structure. The result for $|u_2|^2$ is similar to that for $|u_1|^2$ due to symmetry and hence not shown. The case for a shallower optical lattice (by taking $E_0 = 3.2 \times 10^4$ V cm^{-1}) is also simulated, with the result plotted in Figs. 3(c) and 3(d) for $t = 0$ and $t = 3\tau_0$, respectively. We see that in this case a multiple-peaked soliton appears. In both simulations, $\delta_p = 1.0 \times 10^6$ s^{-1}, $\delta_{c2} = 1.0 \times 10^5$ s^{-1}, and $R_\perp = 16 \ \mu$m with other parameters the same with those in Fig. 1. In addition, $U_0 = 6.8 \times 10^6$ s^{-1}, which allows enough nonlinearity to balance the diffraction. The typical diffraction length L_{Diff} and nonlinearity length L_{Nonl} are around 0.2 cm. Furthermore, B_1 is chosen as zero, that is, the SG gradient magnetic field is absent, thus no SG deflection occurs. We stress that the far-detuned optical lattice laser field is necessary for obtaining a stable propagation of the high-dimensional VOS.

We use two methods to test the stability of the high-dimensional VOS. The first is to add a small random perturbation to the stationary solution obtained in imaginary time [Figs. 3(a) and 3(c)], and evolve the solution in real time [Figs. 3(b) and 3(d)] based on Eq. (13). We found that the soliton can indeed propagate stably for a long time [Figs. 3(b) and 3(d)]. The second is to use a standard linear stability analysis by neglecting small absorption (the absorption length of the system $L_{\text{Abs}} \equiv 1/A_j$ is around 1.8 cm, which is much longer than the diffraction length). Specifically, we add a small perturbation to the stationary solution and solve numerically the eigenvalue problem (see Appendix C) related to the perturbation. We find that all eigenvalues have a vanishing
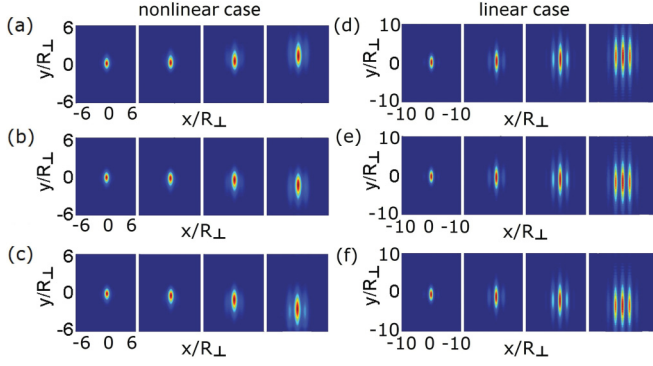
FIG. 4. (Color online) SG effect of ultraslow VOS. (a) and (b) Symmetric deflection (on y axis) of $|u_1|^2$ and $|u_2|^2$ when propagating from $z = 2L_{\mathrm{Diff}}$ to $z = 8L_{\mathrm{Diff}}$ (corresponding respectively to the subfigure from left to right), respectively. (c) Asymmetric deflection of $|u_2|^2$ [$|u_1|^2$ is the same as (a) thus not shown]. (d), (e), and (f) The corresponding evolution of two polarization components in a linear case.

real part, so the VOS is stable against the perturbation with the choice of parameters used in Fig. 3. The physical reason of the stabilization of the VOS is due to the far-detuned optical-lattice field (2) that contributes a trapping potential to the VOS.

IV. STERN-GERLACH EFFECT OF THE VECTOR OPTICAL SOLITONS

Now we investigate the deflection of trajectory of the VOS by numerically simulating Eq. (11) with $B_1 \neq 0$. Shown in Figs. 4(a) and 4(b) are spatial distributions of $|v_1|^2$ [Fig. 4(a)] and $|v_2|^2$ [Fig. 4(b)] in the (x, y) plane when the VOS propagates from $z = 2L_{\mathrm{Diff}}$ to $z = 8L_{\mathrm{Diff}}$ with group velocities $V_{g1} \simeq V_{g2} = 3.2 \times 10^{-6}c$. In the simulation we have chosen $B_1 = 0.7$ mG μm^{-1}. We see that an obvious deflection of VOS trajectories occurs due to the existence of the SG gradient magnetic field. In addition, the two different polarization components deflect symmetrically in opposite (i.e., $+y$ and $-y$) directions, similar to the SG deflection for atoms.

However, in contrast with the atomic SG deflection where trajectories are always symmetric for the two different spin components, the SG deflection of the VOS components can be asymmetric because the two VOS components can propagate with different velocities. To show this we take $\Omega_{c2} = 0.9 \times 10^7$ s^{-1} without changing other parameters, then we have $(V_{g1}, V_{g2}) = (3.2, 2.6) \times 10^{-6}c$. In this situation the σ^- component keeps the same trajectory as Fig. 4(a), whereas the σ^+ component displays a different trajectory against Fig. 4(b). Shown in Fig. 4(c) is the trajectory of the σ^+ component when it propagates from $z = 2L_{\mathrm{Diff}}$ to $z = 8L_{\mathrm{Diff}}$. We see that the deflection in Fig. 4(c) is more significant than that in Fig. 4(b).

For comparison, in Figs. 4(d), 4(e), and 4(f) we present results of corresponding evolution for a linear case (i.e., for a small typical Rabi frequency $U_0 = 6.8 \times 10^5$ s^{-1}). We see that the probe pulse spread rapidly due to diffraction. Thus the nonlinear effect is necessary for balancing the diffraction and hence obtaining the stable VOS and its robust SG deflection.

Analytical VOS solutions of Eq. (13) can be gained by using several reasonable approximations. First, the small absorption term $-iA_j v_j$ is disregarded. Second, since in the presence of the SG gradient magnetic field the two polarization components of the VOS separate each other after propagating some distance, the cross-phase-modulation terms can be neglected. Third, each well of the optical lattice is deep enough, so that the VOS is almost trapped in one well and has single-peaked structure. Hence $V_j(\xi, \eta)$ given by Eq. (12) can be approximated as $\mathcal{M}_j \eta + \mathcal{N}_j(1 - \xi^2)$ and Eq. (13) can be rewritten as

$$\left[\frac{i}{v_{gj}} \frac{\partial}{\partial \tau} + \frac{1}{2} \left(\frac{\partial^2}{\partial \xi^2} + \frac{\partial^2}{\partial \eta^2} \right) \right] v_j - \frac{1}{\sqrt{2\pi}\rho_0} g_{jj}|v_j|^2 v_j$$
$$+ (\mathcal{M}_j \eta + \mathcal{N}_j - \mathcal{N}_j \xi^2) v_j = 0. \tag{14}$$

Taking $v_j(\tau, \xi, \eta) = w_j(\tau, \eta)\phi_j(\xi) \exp[i\mathcal{N}_j v_{gj}\tau]$, where $\phi_j(\xi)$ is the normalized ground state of the eigenvalue problem $(\partial^2/\partial \xi^2 - \mathcal{N}_j \xi^2/2)\phi_j = 2E_\xi \phi_j$ with $E_\xi = -\sqrt{\mathcal{N}_j/2}$, and integrating out the variable ξ, Eq. (14) becomes (see Appendix D for details)

$$\left(\frac{i}{v_{gj}} \frac{\partial}{\partial \tau} + \frac{1}{2} \frac{\partial^2}{\partial \eta^2} \right) w_j - \frac{\mathcal{N}_j^{1/4}}{2^{3/4}\pi\rho_0} g_{jj}|w_j|^2 w_j$$
$$+ \left(\mathcal{M}_j \eta - \frac{\sqrt{\mathcal{N}_j}}{\sqrt{2}} \right) w_j = 0. \tag{15}$$

Equation (15) admits exact soliton solutions [21]. A single-soliton solution reads

$$u_j = A_j \left[1/(\rho_0 \sqrt{\pi}) \right]^{1/2} (\sqrt{2\mathcal{N}_j}/\pi)^{1/4} e^{i\varphi_j} e^{-(s - v_{gj}\tau)^2/(2\rho_0^2)}$$
$$\times e^{-\sqrt{\mathcal{N}_j}\xi^2/\sqrt{2}} \mathrm{sech}\Theta_j, \tag{16}$$

where $A_j = (2^{5/4}\mathcal{N}_j^{1/4}\pi\rho_0/|g_{jj}|)^{1/2}$, $\varphi_j = \mathcal{M}_j v_{gj}\tau(\eta - \mathcal{M}_j v_{gj}^2\tau^2/6)$, and $\Theta_j = (2\mathcal{N}_j)^{1/4}(\eta - \mathcal{M}_j v_{gj}^2\tau^2/2)$ $(j = 1, 2)$. From expression (16) we see that both VOS components are localized in three spatial and one temporal dimensions. Thus (u_1, u_2) can be considered as a *vector optical bullet* due to the localized character in both space and time.

We now estimate the deflection angles of the VOS components. After passing through the medium with length L, the center position of the jth polarization component of the VOS is at $(x, y_j, z) = [0, \mathcal{M}_j L^2 R_\perp/(2L_{\mathrm{diff}}^2), L]$ with the propagating velocity along the z (y) axis given by V_{gj} ($V_j \equiv \mathcal{M}_j v_{gj}^2 R_\perp t/\tau_0^2$). As a result, the expected deflection angle of the output jth polarization component of the VOS after passing through the medium is given by

$$\theta_j = V_j/V_{gj} = (L/V_{gj})(\mu_{\mathrm{sol}\,j}/p)r^2 B_1, \tag{17}$$

where $r = R_\perp/L_{\mathrm{Diff}}$, $p = \hbar k_p$ is photon momentum, and $\mu_{\mathrm{sol}\,j} = M_j V_{gj}\hbar k_p$ is the effective magnetic moment. With the data in Fig. 4 we obtain $\mu_{\mathrm{sol}\,1,2} = \pm 7.6 \times 10^{-20}$ J/T, which is four orders of magnitude larger than the effective magnetic moment for linear polariton obtained in Ref. [4]. From (17) we see the deflection angle of the jth polarization component of the VOS is proportional to the medium length L, the SG gradient magnetic field B_1, and inversely proportional to the group velocity V_{gj}.

In a mechanical viewpoint, the deflection of the jth component of the VOS is caused by the transverse magnetic force $F_j = \mu_{\mathrm{sol}\,j}B_1$ and the deflection angle can be expressed as $\theta_j = F_j t_{\mathrm{int}\,j}r^2/p_j$ with $t_{\mathrm{int}\,j} = L/V_{gj}$ being the interaction
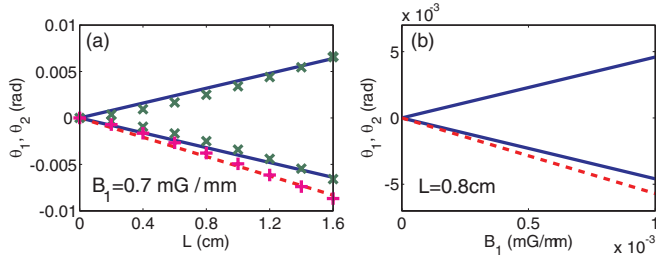
FIG. 5. (Color online) (a) Deflection angles of the VOS as functions of medium length L for magnetic field $B_1 = 0.7 \, \text{mG}/\mu\text{m}$. The solid line with positive (negative) slope is the analytical result of θ_1 (θ_2) for the symmetric case. Dashed line is the analytical result of θ_2 for the asymmetric case (θ_1 is the same as the symmetric case thus not shown). Points labeled by "x" and "+" are center positions of the VOS polarization components obtained numerically. (b) Deflection angles of the VOS as functions of B_1 for $L = 0.8$ cm. The solid line of positive (negative) slope is the result for θ_1 (θ_2) in the symmetric case. Dashed line is the result of θ_2 in the asymmetric case (θ_1 is the same as the symmetric case hence not shown).

time between the probe field and atoms. Notice that due to untraslow propagating velocity of the VOS, large deflection angles may be observed even for very small L.

Shown in Fig. 5(a) are deflection angles of the VOS as functions of medium length L for magnetic field $B_1 = 0.7 \, \text{mG}/\mu\text{m}$. The solid line with positive (negative) slope is the result of θ_1 (θ_2) for the σ^- (σ^+) component, obtained by using the formula (17) with $j = 1$ ($j = 2$) for $V_{g1} \simeq V_{g2} = 3.3 \times 10^{-6}c$ (i.e., the symmetric case). Points labeled by "x" are numerical results of the center position of VOS polarization components obtained in Figs. 4(a) and 4(b). From these results we obtain $(\theta_1, \theta_2) \simeq (3.1, -3.1) \times 10^{-3}$ rad for $L = 4L_{\text{Diff}} = 0.8$ cm, which is two orders of magnitude larger than that for linear polariton obtained in Ref. [4]. In the same figure, the dashed line is the result of θ_2 for $(V_{g1}, V_{g2}) = (3.2, 2.6) \times 10^{-6}c$ (i.e., the asymmetric case), with points labeled by "+" taken from numerical results in Fig. 4(c) (θ_1 is the same as the symmetric case). We see that in both cases analytical results agree well with the numerical ones.

The SG effect of the VOS demonstrated above may have many interesting applications. For example, by measuring the deflection angles of the VOS components, one can obtain the value of the SG gradient magnetic field. Shown in Fig. 5(b) are deflection angles of the VOS components as functions of B_1 for $L = 4L_{\text{Diff}} = 0.8$ cm. The solid line of positive (negative) slope in the figure is the result of θ_1 (θ_2) for the symmetric case. Dashed line is the result of θ_2 for the asymmetric case (θ_1 is the same as the symmetric case thus not shown). Since the deflection angles can be measured easily, one can design an optical magnetometery based on the SG deflection of the VOS.

Using Poynting's vector [13] it is easy to estimate the input power for generating the high-dimensional VOS predicted above, which is estimated as

$$P \approx 3.5 \, \text{nW}. \quad (18)$$

Thus for producing such VOS very low input light intensity is needed. This is a drastic contrast to conventional media

such as glass-based optical fibers, where picosecond or femtosecond laser pulses are usually needed to reach a very high peak power to bring out the enough nonlinear effect required for soliton formation.

V. CONCLUSION

In this work we have proposed a scheme to exhibit SG deflection of high-dimensional VOS via a double EIT. We have shown that the propagating velocity of such VOS may be reduced to $10^{-6} \, c$ and the generation power can be lowered to nanowatt. The stabilization of the VOS can be realized by using a far-detuned optical lattice, and trajectories of them can be deflected significantly by using a SG gradient magnetic field. Deflection angles of the VOS can be of magnitude of 10^{-3} rad when propagating several millimeters. Different from atomic Stern-Gerlach deflection, deflection angles of the VOS can be distinct for different polarization components, and can be manipulated in a controllable way. The result obtained can be described in terms of a SG effect of the VOS with quasispin and effective magnetic moments. We expect that such robust SG effect of light have potential applications in the field of optical magnetometery, quantum information manipulation and storage, and so on.

APPENDIX A: EXPLICIT FORM OF THE BLOCH EQ. (4)

Equations of motion of the density-matrix elements ρ_{jl} are

$$\frac{\partial \rho_{11}}{\partial t} = -i\Omega_{c1}^* \rho_{21} + i\Omega_{c1}\rho_{12} + \Gamma_{41}\rho_{44} + \Gamma_{21}\rho_{22}, \quad (A1a)$$

$$\frac{\partial \rho_{22}}{\partial t} = -i\Omega_{c1}\rho_{12} + i\Omega_{c1}^*\rho_{21} + i\Omega_{p1}^*\rho_{23} - i\Omega_{p1}\rho_{32} - \Gamma_2\rho_{22}, \quad (A1b)$$

$$\frac{\partial \rho_{33}}{\partial t} = -i\Omega_{p1}^*\rho_{23} + i\Omega_{p1}\rho_{32} + i\Omega_{p2}\rho_{34} - i\Omega_{p2}^*\rho_{43} + \Gamma_{43}\rho_{44} + \Gamma_{23}\rho_{22}, \quad (A1c)$$

$$\frac{\partial \rho_{44}}{\partial t} = -i\Omega_{p2}\rho_{34} + i\Omega_{p2}^*\rho_{43} + i\Omega_{c2}^*\rho_{45} - i\Omega_{c2}\rho_{54} - \Gamma_4\rho_{44}, \quad (A1d)$$

$$\frac{\partial \rho_{55}}{\partial t} = -i\Omega_{c2}^*\rho_{45} + i\Omega_{c2}\rho_{54} + \Gamma_{45}\rho_{44} + \Gamma_{25}\rho_{22}, \quad (A1e)$$

for diagonal elements, and

$$\frac{\partial \rho_{12}}{\partial t} = i\delta_{c1}\rho_{12} - i\Omega_{c1}^*(\rho_{22} - \rho_{11}) + i\Omega_{p1}^*\sigma_{13} - \frac{\Gamma_2 + \gamma_{12}}{2}\rho_{12}, \quad (A2a)$$

$$\frac{\partial \rho_{13}}{\partial t} = i(\delta_{c1} - \delta_p)\rho_{13} + i\Omega_{p1}\rho_{12} + i\Omega_{p2}\rho_{14} - i\Omega_{c1}^*\rho_{23} - \frac{\gamma_{13}}{2}\rho_{13}, \quad (A2b)$$

$$\frac{\partial \rho_{14}}{\partial t} = i(\Delta + \delta_{c1})\rho_{14} + i\Omega_{p2}^* \rho_{13} + i\Omega_{c2}^* \rho_{15} - i\Omega_{c1}^* \rho_{24}$$
$$- \frac{\Gamma_4 + \gamma_{14}}{2}\rho_{14}, \tag{A2c}$$

$$\frac{\partial \rho_{15}}{\partial t} = i(\Delta + \delta_{c1} - \delta_{c2})\rho_{15} + i\Omega_{c2}\rho_{14} - i\Omega_{c1}^* \rho_{25} - \frac{\gamma_{15}}{2}\rho_{15}, \tag{A2d}$$

$$\frac{\partial \rho_{23}}{\partial t} = -i\delta_p \rho_{23} - i\Omega_{c1}\rho_{13} + i\Omega_{p2}\rho_{24} - i\Omega_{p1}(\rho_{33} - \rho_{22})$$
$$- \frac{\Gamma_2 + \gamma_{23}}{2}\rho_{23}, \tag{A2e}$$

$$\frac{\partial \rho_{24}}{\partial t} = i\Delta \rho_{24} - i\Omega_{c1}\rho_{14} + i\Omega_{c2}^* \rho_{25} + i\Omega_{p2}^* \rho_{23} - i\Omega_{p1}\rho_{34}$$
$$- \frac{\Gamma_2 + \Gamma_4 + \gamma_{24}}{2}\rho_{24}, \tag{A2f}$$

$$\frac{\partial \rho_{25}}{\partial t} = i(\Delta - \delta_{c2})\rho_{25} - i\Omega_{c1}\rho_{15} - i\Omega_{p1}\rho_{35} + i\Omega_{c2}\rho_{24}$$
$$- \frac{\Gamma_2 + \gamma_{25}}{2}\rho_{25}, \tag{A2g}$$

$$\frac{\partial \rho_{34}}{\partial t} = i(\delta_p + \Delta)\rho_{34} - i\Omega_{p1}^* \rho_{24} + i\Omega_{c2}^* \rho_{35} - i\Omega_{p2}^*(\rho_{44} - \rho_{33})$$
$$- \frac{\Gamma_4 + \gamma_{34}}{2}\rho_{34}, \tag{A2h}$$

$$\frac{\partial \rho_{35}}{\partial t} = i(\delta_p + \Delta - \delta_{c2})\rho_{35} - i\Omega_{p1}^* \rho_{25} - i\Omega_{p2}^* \rho_{45} + i\Omega_{c2}\rho_{34}$$
$$- \frac{\gamma_{35}}{2}\rho_{35}, \tag{A2i}$$

$$\frac{\partial \rho_{45}}{\partial t} = -i\delta_{c2}\rho_{45} - i\Omega_{c2}(\rho_{55} - \rho_{44}) - i\Omega_{p2}\rho_{35} - \frac{\Gamma_4 + \gamma_{45}}{2}\rho_{45}, \tag{A2j}$$

for nondiagonal elements. Here $\Gamma_2 = \Gamma_{12} + \Gamma_{32} + \Gamma_{52}$ and $\Gamma_4 = \Gamma_{14} + \Gamma_{34} + \Gamma_{54}$ are decay rates, with Γ_{jl} being the spontaneous emission decay rate from state $|l\rangle$ to state $|j\rangle$. $\gamma_{jl} = (\Gamma_j + \Gamma_l)/2 + \gamma_{jl}^{\text{col}}$, with γ_{jl}^{col} the dephasing rates related to states $|j\rangle$ and $|l\rangle$.

APPENDIX B: ASYMPTOTIC EXPANSION OF THE MAXWELL-BLOCH EQUATIONS

The asymptotic expansions of the Bloch equations read

$$i\frac{\partial}{\partial t_0}\rho_{11}^{(l)} - \Omega_{c1}^* \rho_{21}^{(l)} + \Omega_{c1}\rho_{12}^{(l)} - i\Gamma_{41}\rho_{44}^{(l)} - i\Gamma_{21}\rho_{22}^{(l)} = A^{(l)}, \tag{B1a}$$

$$\left(i\frac{\partial}{\partial t_0} + i\Gamma_2\right)\rho_{22}^{(l)} - \Omega_{c1}\rho_{12}^{(l)} + \Omega_{c1}^* \rho_{21}^{(l)} = B^{(l)}, \tag{B1b}$$

$$\left(i\frac{\partial}{\partial t_0} + i\Gamma_4\right)\rho_{44}^{(l)} + \Omega_{c2}^* \rho_{45}^{(l)} - \Omega_{c2}\rho_{54}^{(l)} = C^{(l)}, \tag{B1c}$$

$$i\frac{\partial}{\partial t_0}\rho_{55}^{(l)} - \Omega_{c2}^* \rho_{45}^{(l)} + \Omega_{c2}\rho_{54}^{(l)} - i\Gamma_{45}\rho_{44}^{(l)} - i\Gamma_{25}\rho_{22}^{(l)} = D^{(l)}, \tag{B1d}$$

for the diagonal matrix elements, and

$$\left(i\frac{\partial}{\partial t_0} + \delta_{c1}^{(0)} + i\frac{\Gamma_2 + \gamma_{12}}{2}\right)\rho_{12}^{(l)} - \Omega_{c1}^*\left(\rho_{22}^{(l)} - \rho_{11}^{(l)}\right) = E^{(l)}, \tag{B2a}$$

$$\left(i\frac{\partial}{\partial t_0} + \delta_{c1}^{(0)} - \delta_p^{(0)} + i\frac{\gamma_{13}}{2}\right)\rho_{13}^{(l)} - \Omega_{c1}^* \rho_{23}^{(l)} = F^{(l)}, \tag{B2b}$$

$$\left(i\frac{\partial}{\partial t_0} + \Delta^{(0)} + \delta_{c1}^{(0)} + i\frac{\Gamma_4 + \gamma_{14}}{2}\right)\rho_{14}^{(l)} - \Omega_{c1}^* \rho_{24}^{(l)} + \Omega_{c2}^* \rho_{15}^{(l)}$$
$$= G^{(l)}, \tag{B2c}$$

$$\left(i\frac{\partial}{\partial t_0} + \Delta^{(0)} + \delta_{c1}^{(0)} - \delta_{c2}^{(0)} + i\frac{\gamma_{15}}{2}\right)\rho_{15}^{(l)} - \Omega_{c1}^* \rho_{25}^{(l)} + \Omega_{c2}\rho_{14}^{(l)}$$
$$= H^{(l)}, \tag{B2d}$$

$$\left(i\frac{\partial}{\partial t_0} - \delta_p^{(0)} + i\frac{\Gamma_2 + \gamma_{23}}{2}\right)\rho_{23}^{(l)} - \Omega_{c1}\rho_{13}^{(l)} - \Omega_{p1}^{(l)} = I^{(l)}, \tag{B2e}$$

$$\left(i\frac{\partial}{\partial t_0} + \Delta^{(0)} + i\frac{\Gamma_2 + \Gamma_4 + \gamma_{24}}{2}\right)\rho_{24}^{(l)} - \Omega_{c1}\rho_{14}^{(l)} + \Omega_{c2}^* \rho_{25}^{(l)}$$
$$= J^{(l)}, \tag{B2f}$$

$$\left(i\frac{\partial}{\partial t_0} + \Delta^{(0)} - \delta_{c2}^{(0)} + i\frac{\Gamma_2 + \gamma_{25}}{2}\right)\rho_{25}^{(l)} - \Omega_{c1}\rho_{15}^{(l)} + \Omega_{c2}\rho_{24}^{(l)}$$
$$= K^{(l)}, \tag{B2g}$$

$$\left(i\frac{\partial}{\partial t_0} + \delta_p^{(0)} + \Delta^{(0)} + i\frac{\Gamma_4 + \gamma_{34}}{2}\right)\rho_{34}^{(l)} + \Omega_{c2}^* \rho_{35}^{(l)} + \Omega_{p2}^{*(l)}$$
$$= L^{(l)}, \tag{B2h}$$

$$\left(i\frac{\partial}{\partial t_0} + \delta_p^{(0)} + \Delta^{(0)} - \delta_{c2}^{(0)} + i\frac{\gamma_{35}}{2}\right)\rho_{35}^{(l)} + \Omega_{c2}\rho_{34}^{(l)} = M^{(l)}, \tag{B2i}$$

$$\left(i\frac{\partial}{\partial t_0} - \delta_{c2}^{(0)} + i\frac{\Gamma_4 + \gamma_{45}}{2}\right)\rho_{45}^{(l)} - \Omega_{c2}\left(\rho_{55}^{(l)} - \rho_{44}^{(l)}\right) = N^{(l)}, \tag{B2j}$$

for the nondiagonal elements. The equation for ρ_{33} has been replaced by the closed system condition $\sum_{j=1}^{5}\rho_{jj} = 1$, that is, $\sum_{j=1}^{5}\rho_{jj}^{(l)} = 0$ ($l \geqslant 1$). The asymptotic expansion of the Maxwell equation is

$$i\left(\frac{\partial}{\partial z_0} + \frac{1}{c}\frac{\partial}{\partial t_0}\right)\Omega_{p1}^{(l)} - \kappa_{32}\rho_{23}^{(l)} = O^{(l)}, \tag{B3a}$$

$$i\left(\frac{\partial}{\partial z_0} + \frac{1}{c}\frac{\partial}{\partial t_0}\right)\Omega_{p2}^{(l)} - \kappa_{34}\rho_{43}^{(l)} = P^{(l)}. \tag{B3b}$$

The quantities on the right-hand side of Eqs. (B1)–(B3) are given as $A^{(1)} = B^{(1)} = C^{(1)} = D^{(1)} = E^{(1)} = F^{(1)} = G^{(1)} = H^{(1)} = I^{(1)} = J^{(1)} = K^{(1)} = L^{(1)} = M^{(1)} = N^{(1)} = O^{(1)} = P^{(1)} = A^{(2)} = D^{(2)} = H^{(2)} = O^{(2)} = P^{(2)} = 0$, $B^{(2)} = -\Omega_{p1}^{*(1)}\rho_{23}^{(1)} + \Omega_{p1}^{(1)}\rho_{32}^{(1)}$, $C^{(2)} = \Omega_{p2}^{(1)}\rho_{34}^{(1)} - \Omega_{p2}^{*(1)}\rho_{43}^{(1)}$, $E^{(2)} = -\Omega_{p1}^{*(1)}\rho_{13}^{(1)}$, $F^{(2)} = -\Omega_{p2}^{(1)}\rho_{14}^{(1)} - \Omega_{p1}^{(1)}\rho_{12}^{(1)}$, $G^{(2)} = -\Omega_{p2}^{(1)}\rho_{13}^{(1)}$, $I^{(2)} = -\Omega_{p2}^{(1)}\rho_{24}^{(1)} + \Omega_{p1}^{(1)}(\rho_{33}^{(1)} - \rho_{22}^{(1)})$, $J^{(2)} = -\Omega_{p2}^{*(1)}\rho_{23}^{(1)} + \Omega_{p1}^{(1)}\rho_{34}^{(1)}$, $K^{(2)} = \Omega_{p1}^{(1)}\rho_{35}^{(1)}$, $L^{(2)} = \Omega_{p1}^{*(1)}\rho_{24}^{(1)} + \Omega_{p2}^{*(1)}(\rho_{44}^{(1)} - \rho_{33}^{(1)})$, $M^{(2)} = \Omega_{p2}^{*(1)}\rho_{45}^{(1)} +$

$\Omega_{p1}^{*(1)}\rho_{25}^{(1)}$, $N^{(2)}=\Omega_{p2}^{(1)}\rho_{35}^{(1)}$, and

$$A^{(3)}=-i\frac{\partial\rho_{11}^{(1)}}{\partial t_2},\quad D^{(3)}=-i\frac{\partial\rho_{55}^{(1)}}{\partial t_2},$$

$$B^{(3)}=-i\frac{\partial}{\partial t_2}\rho_{22}^{(1)}-\Omega_{p1}^{*(2)}\rho_{23}^{(1)}-\Omega_{p1}^{*(1)}\rho_{23}^{(2)}+\Omega_{p1}^{(2)}\rho_{32}^{(1)}$$
$$+\Omega_{p1}^{(1)}\rho_{32}^{(2)},$$

$$C^{(3)}=-i\frac{\partial}{\partial t_2}\rho_{44}^{(1)}+\Omega_{p2}^{(2)}\rho_{34}^{(1)}+\Omega_{p2}^{(1)}\rho_{34}^{(2)}-\Omega_{p2}^{*(2)}\rho_{43}^{(1)}$$
$$-\Omega_{p2}^{*(1)}\rho_{43}^{(2)},$$

$$E^{(3)}=-\left(i\frac{\partial}{\partial t_2}+\delta_{c1}^{(2)}\right)\rho_{12}^{(1)}-\Omega_{p1}^{*(2)}\rho_{13}^{(1)}-\Omega_{p1}^{*(1)}\rho_{13}^{(2)},$$

$$F^{(3)}=-\left(i\frac{\partial}{\partial t_2}+\delta_{c1}^{(2)}-\delta_{p}^{(2)}\right)\rho_{13}^{(1)}-\Omega_{p2}^{(2)}\rho_{14}^{(1)}-\Omega_{p2}^{(1)}\rho_{14}^{(2)}$$
$$-\Omega_{p1}^{(2)}\rho_{12}^{(1)}-\Omega_{p1}^{(1)}\rho_{12}^{(2)},$$

$$G^{(3)}=-\left(i\frac{\partial}{\partial t_2}+\Delta^{(2)}+\delta_{c1}^{(2)}\right)\rho_{14}^{(1)}+\Omega_{p2}^{(2)}\rho_{13}^{(1)}+\Omega_{p2}^{(1)}\rho_{13}^{(2)}$$
$$-\Omega_{p2}^{*(2)}\rho_{13}^{(1)}-\Omega_{p2}^{*(1)}\rho_{13}^{(2)},$$

$$H^{(3)}=-\left(i\frac{\partial}{\partial t_2}+\Delta^{(2)}+\delta_{c1}^{(2)}-\delta_{c2}^{(2)}\right)\rho_{15}^{(1)},$$

$$I^{(3)}=-\left(i\frac{\partial}{\partial t_2}-\delta_{p}^{(2)}\right)\rho_{23}^{(1)}-\Omega_{p2}^{(2)}\rho_{24}^{(1)}-\Omega_{p2}^{(1)}\rho_{24}^{(2)}+\Omega_{p1}^{(2)}$$
$$\times\left(\rho_{33}^{(1)}-\rho_{22}^{(1)}\right)+\Omega_{p1}^{(1)}\left(\rho_{33}^{(2)}-\rho_{22}^{(2)}\right),$$

$$J^{(3)}=-\left(i\frac{\partial}{\partial t_2}+\Delta^{(2)}\right)\rho_{24}^{(1)}-\Omega_{p2}^{*(2)}\rho_{23}^{(1)}-\Omega_{p2}^{*(1)}\rho_{23}^{(2)}$$
$$+\Omega_{p1}^{(2)}\rho_{34}^{(1)}+\Omega_{p1}^{(1)}\rho_{34}^{(2)},$$

$$K^{(3)}=-\left(i\frac{\partial}{\partial t_2}+\Delta^{(2)}-\delta_{c2}^{(2)}\right)\rho_{25}^{(1)}+\Omega_{p1}^{(2)}\rho_{35}^{(1)}+\Omega_{p1}^{(1)}\rho_{35}^{(2)},$$

$$L^{(3)}=-\left(i\frac{\partial}{\partial t_2}+\delta_{p}^{(2)}+\Delta^{(2)}\right)\rho_{34}^{(1)}+\Omega_{p1}^{*(2)}\rho_{24}^{(1)}+\Omega_{p1}^{*(1)}\rho_{24}^{(2)}$$
$$+\Omega_{p2}^{*(2)}\left(\rho_{44}^{(1)}-\rho_{33}^{(1)}\right)+\Omega_{p2}^{*(1)}\left(\rho_{44}^{(2)}-\rho_{33}^{(2)}\right),$$

$$M^{(3)}=-\left(i\frac{\partial}{\partial t_2}+\delta_{p}^{(2)}+\Delta^{(2)}-\delta_{c2}^{(2)}\right)\rho_{35}^{(1)}+\Omega_{p2}^{*(2)}\rho_{45}^{(1)}$$
$$+\Omega_{p2}^{*(1)}\rho_{45}^{(2)}+\Omega_{p1}^{*(2)}\rho_{25}^{(1)}+\Omega_{p1}^{*(1)}\rho_{25}^{(2)},$$

$$N^{(3)}=-\left(i\frac{\partial}{\partial t_2}-\delta_{c2}^{(2)}\right)\rho_{45}^{(1)}+\Omega_{p2}^{(2)}\rho_{35}^{(1)}+\Omega_{p2}^{(1)}\rho_{35}^{(2)},$$

$$O^{(3)}=-i\left(\frac{\partial}{\partial z_2}+\frac{1}{c}\frac{\partial}{\partial t_2}\right)\Omega_{p1}^{(1)}-\frac{c}{2\omega_p}\left(\frac{\partial^2}{\partial x_1^2}+\frac{\partial^2}{\partial y_1^2}\right)\Omega_{p1}^{(1)},$$

$$P^{(3)}=-i\left(\frac{\partial}{\partial z_2}+\frac{1}{c}\frac{\partial}{\partial t_2}\right)\Omega_{p2}^{(1)}-\frac{c}{2\omega_p}\left(\frac{\partial^2}{\partial x_1^2}+\frac{\partial^2}{\partial y_1^2}\right)\Omega_{p2}^{(1)}.$$

APPENDIX C: EIGENVALUE PROBLEM FOR THE STABILITY OF VOS

We consider a small perturbation adding to the stationary VOS solution, that is,

$$v_j(\tau,\xi,\eta)=\{v_{\text{st}\,j}(\xi,\eta)+[\sigma_j(\xi,\eta)+\varsigma_j(\xi,\eta)]e^{\lambda\tau}$$
$$+[\sigma_j^*(\xi,\eta)-\varsigma_j^*(\xi,\eta)]e^{\lambda^*\tau}\}e^{i\mu_j\tau},\quad\text{(C1)}$$

where $(v_{\text{st}1},v_{\text{st}2})$ is a stationary solution, $\sigma_j(\xi,\eta)$ and $\varsigma_j(\xi,\eta)$ are normal modes, μ_j are frequencies, and λ is the eigenvalue. Substituting (C1) into Eq. (13), one obtains the linear eigenvalue equations related to the perturbation

$$i\frac{\lambda}{v_{g1}}\sigma_1+\left(\frac{1}{2}\nabla_\perp^2+V_1(\xi,\eta)-\frac{\mu_1}{v_{g1}}\right)\varsigma_1-g_{11}v_{\text{st}1}^2\varsigma_1$$
$$-g_{12}v_{\text{st}2}^2\varsigma_1=0,\quad\text{(C2a)}$$

$$i\frac{\lambda}{v_{g1}}\varsigma_1+\left(\frac{1}{2}\nabla_\perp^2+V_1(\xi,\eta)-\frac{\mu_1}{v_{g1}}\right)\sigma_1-3g_{11}v_{\text{st}1}^2\sigma_1$$
$$-g_{12}\left(v_{\text{st}2}^2\sigma_1+2v_{\text{st}1}v_{\text{st}2}\sigma_2\right)=0,\quad\text{(C2b)}$$

$$i\frac{\lambda}{v_{g2}}\sigma_2+\left(\frac{1}{2}\nabla_\perp^2+V_2(\xi,\eta)-\frac{\mu_2}{v_{g2}}\right)\varsigma_2-g_{22}v_{\text{st}2}^2\varsigma_2$$
$$-g_{21}v_{\text{st}1}^2\varsigma_2=0,\quad\text{(C2c)}$$

$$i\frac{\lambda}{v_{g2}}\varsigma_2+\left(\frac{1}{2}\nabla_\perp^2+V_2(\xi,\eta)-\frac{\mu_2}{v_{g2}}\right)\sigma_2-3g_{22}v_{\text{st}2}^2\sigma_2$$
$$-g_{21}\left(v_{\text{st}1}^2\sigma_2+2v_{\text{st}1}v_{\text{st}2}\sigma_1\right)=0,\quad\text{(C2d)}$$

where $\nabla_\perp^2=\partial_\xi^2+\partial_\eta^2$. The eigenvalue problem (A) can be numerically solved by the finite-difference method.

APPENDIX D: DERIVATION OF ANALYTICAL SOLITON SOLUTIONS

Equation (14) is a $(3+1)$-dimensional nonlinear one with variable coefficients. We can reduce its dimensionality related to the variable ξ by assuming $v_j(\tau,\xi,\eta)=w_j(\tau,\eta)\phi_j(\xi)e^{i\mathcal{N}_j v_{gj}\tau}$, where $\phi_j(\xi)$ is the normalized eigenfunction of the eigenvalue problem

$$\frac{1}{2}\left(\frac{\partial^2}{\partial\xi^2}-\frac{\mathcal{N}_j}{2}\xi^2\right)\phi_j=E_\xi\phi_j,\quad\int_{-\infty}^{\infty}|\phi_j|^2d\xi=1,\quad\text{(D1)}$$

with E_ξ being the eigenvalue. When the optical lattice potential is deep, we can take

$$\phi_j=\sqrt[4]{\frac{\sqrt{2\mathcal{N}_j}}{\pi}}e^{-\sqrt{\frac{\mathcal{N}_j}{2}}\xi^2},\quad\text{(D2)}$$

with $E_\xi=-\sqrt{\mathcal{N}_j/2}$, that is, ϕ_j is a normalized ground state solution. By inserting $v_j(\tau,\xi,\eta)=w_j(\tau,\eta)\phi_j(\xi)e^{i\mathcal{N}_j v_{gj}\tau}$ into Eq. (14) and integrating out the variable ξ, we obtain the equation of w_j:

$$\left(\frac{i}{v_{gj}}\frac{\partial}{\partial\tau}+\frac{1}{2}\frac{\partial^2}{\partial\eta^2}\right)w_j-\frac{\mathcal{N}_j^{1/4}}{2^{3/4}\pi\rho_0}g_{jj}|w_j|^2w_j$$
$$+\left(\mathcal{M}_j\eta-\frac{\sqrt{\mathcal{N}_j}}{\sqrt{2}}\right)w_j=0,\quad\text{(D3)}$$

which is Eq. (15) in the main text. Equation (D3) admits the following exact single-soliton solution [21]

$$w_j=A_je^{i\varphi_j}\text{sech}\,\Theta_j,\quad\text{(D4)}$$

where $A_j=(2^{5/4}\mathcal{N}_j^{1/4}\pi\rho_0/|g_{jj}|)^{1/2}$, $\varphi_j=\mathcal{M}_jv_{gj}\tau(\eta-\mathcal{M}_jv_{gj}^2\tau^2/6)$, and $\Theta_j=(2\mathcal{N}_j)^{1/4}(\eta-\mathcal{M}_jv_{gj}^2\tau^2/2)$. Finally, we obtain the soliton solution (16) given in the main text.

[1] J. J. Sakurai, *Modern Quantum Mechanics*, revised edition (Addison-Wesley, Reading, MA, 1994).

[2] M. D. Girardeau and M. Olshanii, Phys. Rev. A **70**, 023608 (2004).

[3] Y. Li, C. Bruder, and C. P. Sun, Phys. Rev. Lett. **99**, 130403 (2007).

[4] L. Karpa and M. Weitz, Nat. Phys. **2**, 332 (2006).

[5] M. Fleischhauer, A. Imamoglu, and J. P. Marangos, Rev. Mod. Phys. **77**, 633 (2005).

[6] R. Schlesser and A. Weis, Opt. Lett. **17**, 1015 (1992).

[7] R. Holzner, P. Eschle, S. Dangel, R. Richard, H. Schmid, U. Rusch, B. Röhricht, R. J. Ballagh, A. W. McCord, and W. J. Sandle, Phys. Rev. Lett. **78**, 3451 (1997).

[8] G. T. Purves, G. Jundt, and C. S. Adams, Eur. Phys. J. D **29**, 433 (2004).

[9] D. L. Zhou, L. Zhou, R. Q. Wang, S. Yi, and C. P. Sun, Phys. Rev. A **76**, 055801 (2007).

[10] Y. Guo, L. Zhou, L. M. Kuang, and C. P. Sun, Phys. Rev. A **78**, 013833 (2008).

[11] H. R. Zhang, L. Zhou, and C. P. Sun, Phys. Rev. A **80**, 013812 (2009).

[12] Y. Wu and L. Deng, Phys. Rev. Lett. **93**, 143904 (2004).

[13] G. Huang, L. Deng, and M. G. Payne, Phys. Rev. E **72**, 016617 (2005).

[14] C. Hang, G. Huang, and L. Deng, Phys. Rev. E **73**, 036607 (2006).

[15] H. Michinel, M. J. Paz-Alonso, and V. M. Pérez-García, Phys. Rev. Lett. **96**, 023903 (2006).

[16] C. Hang, V. V. Konotop, and G. Huang, Phys. Rev. A **79**, 033826 (2009).

[17] Y. Zhang, Z. Wang, Z. Nie, C. Li, H. Chen, K. Lu, and M. Xiao, Phys. Rev. Lett. **106**, 093904 (2011).

[18] H. J. Li, Y. P. Wu, and G. Huang, Phys. Rev. A **84**, 033816 (2011).

[19] B. B. Baizakov, B. A. Malomed, and M. Salerno, Phys. Rev. A **70**, 053613 (2004).

[20] The frequency of the probe field is $\omega_p + \omega$, and the wave vectors of the jth polarization component is $k_p + K_{pj}(\omega)$. Thus $\omega = 0$ corresponds to the center frequency of the probe field.

[21] J. Yan *et al.*, Phys. Fluids A **4**, 690 (1992).